Parameters deterioration rules of surrounding rock for deep tunnel excavation based on unloading effect

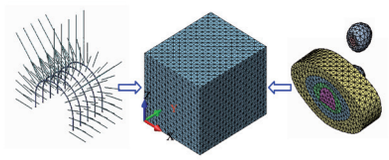

Recomendaciones basadas en el efecto descarga sobre los parámetros de deterioro de las rocas circundantes para la excavación de túneles profundos

Tao Luo[1,2], Shuren Wang[1,3*], Chengguo Zhang[3] and Xiliang Liu[1]

[1] International Joint Research Laboratory of Henan Province for Underground Space Development and Disaster Prevention, Henan Polytechnic University, Jiaozuo, 454003, Henan, China, w_sr88@163.com
[2] College of Resource Engineering, Longyan University, Longyan, 364012, Fujian, China
[3] School of Mining Engineering, University of New South Wales, Sydney, 2052, NSW, Australia

DOI: http://dx.doi.org/10.6036/8554 | Recibido: 04/08/2017 • Evaluado: 04/08/2017 • Aceptado: 10/10/2017

RESUMEN

- El cómo asegurar la seguridad de la construcción es uno de los problemas clave para la excavación de túneles profundos. Ya que la excavación de un túnel es en esencia un proceso de descarga, se puso en práctica un nuevo método para evaluar con precisión para evaluar el daño sobre las rocas circundantes y estudiar el mecanismo de deformación y fallo del tunel, considerando el efecto descarga. Se consideró como aplicación un tunel típico en Shimen Mine (China) para el que se generó un modelo informático de tres dimensiones utilizando la técnica FLAC3D. Entonces se determinaron las diferentes zonas de descarga de la roca circundante de acuerdo con el principio de descarga de la excavación del túnel. Los resultados muestran que los parámetros mecánicos para las diferentes zonas de descarga, como la cohesión, el ángulo de fricción interna, el módulo de elasticidad y la relación de Poisson, presentan características de degradación no lineales. Y se puede encontrar que el rango de incremento del índice de respuesta mecánica, como el desplazamiento, la tensión y la fuerza, aumentan de 0,73 a 2,10 veces, comparando el análisis convencional con el cálculo por descarga. El efecto descarga tiene gran influencia en el concepto de tensión, de desplazamiento y de fuerzas a soportar durante la excavación del túnel. Por eso es más práctico considerar el efecto descarga durante la excavación de un túnel profundo. Las conclusiones obtenidas en el estudio son de un valor teórico importante para orientar prácticas de ingeniería similares.
- **Palabras clave:** Carreteras Profundas, Rocas Circundantes, Efecto Descarga, Mecanismo de Deformación, Parámetros Mecánicos.

ABSTRACT

How to ensure the construction safety is one of the key problems for the deep tunnel excavation. Since a tunnel excavation is an unloading process in essence, a novel method to accurately evaluate the damage evolution of the surrounding rock was conducted to study the deformation and failure mechanism of the tunnel by considering the unloading effect. A typical tunnel in Shimen Mine in China was regarded as the background, the three-dimension computational model was built by using FLAC3D technique. Then the different unloading zones of the surrounding rock were determined according to the unloading principle of tunnel excavation. The results show that the mechanical parameters for the different unloading zones, such as cohesion, internal friction angle, elastic modulus, and Poisson's ratio, display the nonlinear degradation characteristics. And it can be found that the increasing range of the mechanical response index, such as displacement, stress and force, increase about 0.73-2.10 times comparing the conventional analysis with the unloading calculation. The unloading effect has a great influence on the stress field, the displacement field, and the forces of the supporting during the tunnel excavation. So it is more practical to consider the unloading effect during the deep tunnel excavation. The conclusions obtained in the study are of important theoretical value to direct the similar engineering practice.

Keywords: Deep tunnel, Surrounding rock, Unloading effect, Deformation mechanism, Mechanical parameter.

1. INTRODUCTION

According to the statistics, the roof falling accidents are the most frequently fatal accidents in tunnel engineering in China, and there are about 30-40 % of these accidents happen during the process of the tunnel construction [1]. With the increase of the construction depth, the phenomena of large deformation and instability of deep tunnels become more prominent. Besides, the supporting cost of tunnel and the recovery rate become high. Therefore, one of the key problems is how to ensure the construction safety after the tunnel excavation under the high stress conditions.

The tunnel excavation under the high stress conditions is always accompanied by the release of the stress. At the same time, the mechanical parameters of the surrounding rock of the tunnel also experience a complicated mechanical evolution process. The excavation of the tunnel usually causes the stress disturbance and adjustment of the surrounding rock, resulting in the secondary stress field, which is the mechanical process of unloading. Meanwhile, the mechanical parameters of the surrounding rock, such as cohesion, internal friction angle, elastic modulus, and Poisson's ratio will change with the variation of unloading process [2]. According to the traditional numerical analysis of rock mechanics, the mechanical parameters used to remain unchanged states. So it is often regarded as a static process, which is not consistent with the process of the unloading mechanics. And the excavation process of tunnels in this way can not reflect the actual mechanical properties of the surrounding rock if the unloading effect is not considered.

The mechanical parameters of the surrounding rock of the tunnel become degraded because of the further damage caused

by the excavation unloading, which has different changing rules in the different unloading zones. Therefore, for revealing the deformation and failure mechanism after the tunnel excavation, it is necessary to divide different unloading zones according to the unloading conditions and to research the deterioration rules of the mechanical parameters during the deep tunnel excavation.

2. STATE OF THE ART

For the surrounding rock damage caused by the tunnel excavation, lots of scholars have conducted many studies and achieved a great progress about excavation damage of a tunnel. For example, F. Varas, et al. conducted a study of bifurcation in the problem of unloading a circular excavation in a strain-softening rock mass [3]. M. Cai & P.K. Kaiser. presented numerical examples using field monitoring data from a tunnel in granite to demonstrate the micro-seismicity being linked to the dynamic rock properties [4]. L. Malmgren, et al. investigated the excavation disturbed zone at an underground iron ore mine in Sweden using the seismic measurement techniques [5]. S. Kwon, et al. completed an investigation of the excavation damaged zone at the underground research tunnel in Korea [6]. J. Wassermann, et al. monitored the excavation damaged zone in fractured gneisses of the Rose lend tunnel in French [7]. H. Fattahi, et al. used the fuzzy extent analysis method to assess the excavation damage zone of a tunnel in Iran [8]. T. Siren et al. completed several tests to observe the stress-induced and construction-induced excavation damage zone of the tunnel in crystalline rock [9]. The reliability analysis of a circular tunnel in elastic-strain-softening rock mass was analyzed considering the dilatancy angle variation with softening parameter in different stress conditions [10]. Assuming a damageable visco-elasto-plastic argillite skeleton saturated by water, a tunnel located in an underground laboratory in France was excavated to simulate the creep phenomena [11]. but they did not consider the mechanical parameters degradation during the tunnel excavation.

Although the related research on the deep tunnel started relatively late in China, a large number of achievements about the deformation and failure mechanism after a tunnel excavation have been gained for the recent years [12]. For example, H.P. Xie et al. put forward the overall failure criterion of the rock strength based on the principle of energy dissipation and release [13]. M.Y. Wang et al. studied the tectonic deformation and failure of deep rock mass and suggested some related scientific problems [14]. J.C. Gu et al. conducted a model experiment on the deformation characteristics and failure mechanism of the layered fracture of the deep tunnel excavation, they found that the structure of the layered rock mass are closely related to the stress state in the deep tunnel [15]. W.P. Wu et al. analyzed the occurrence mechanism and provided the control strategy of various failure models based on the tunnel damage phenomenon in Jingping in China [16]. J. Li et al. researched on the stress distribution, deformation, and the partition fracturing mechanism of the surrounding rock of the deep tunnel excavation by using the elastic constitutive model [17]. X.X. Liu et al. found that there are some relationships between the horizontal stress and the fracture model for the deep tunnel excavation by the laboratory test [18]. Similarly, they also did not pay attention to the mechanical parameters degradation for the tunnel excavation.

To sum up the above mentioned literatures, we found that many important results had been achieved about the deformation and failure mechanism of the tunnel excavation. However, it was not perfect enough about the mechanical parameters degradation of the surrounding rock caused by the tunnel excavation. So the further study was to be conducted to analyze the failure mechanism of the different unloading zones after the tunnel excavation and to reveal the nonlinear degradation rules of main mechanical parameters for the different unloading zones. The remainder of this study was organized as follows. In Section 3, the research method was introduced. In Section 4, the computational model was built and the different unloading zones of the surrounding rocks were determined. Then, the nonlinear degradation laws of four mechanical parameters for the different unloading zones were revealed. Finally, some conclusions were given in Section 5.

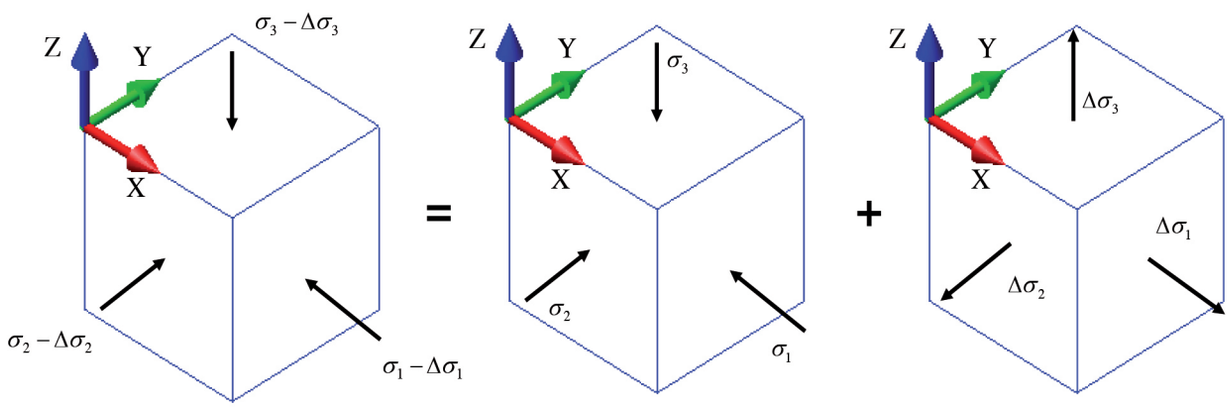

Fig. 1: Schematic diagram of three-dimension unloading effect

3. METHODOLOGY

3.1. UNLOADING PRINCIPLE OF TUNNEL EXCAVATION

As shown in Fig. 1, the unloading effect is equal to add three tensile stress in the opposite direction to the initial stress field of the rock mass unit. Thus, the unloading stress (displacement) field of the tunnel excavation can be decomposed into two parts of the model: the initial stress (displacement) field before the tunnel excavation and the unloading stress (displacement) field caused by the tunnel excavation.

The numerical simulation of excavation unloading is as follows:

Step 1: Calculating the initial stress (displacement) field. The initial stress (displacement) field can be obtained after the initial stress field σ_0 (MPa) and the initial displacement field μ_0 (mm) are calculated. The initial displacement is set to zero before tunnel

excavation, so that we can get the displacement characteristics caused by the tunnel unloading excavation.

Step 2: There is the superposition stress (displacement) field for the first unloading. The stress field σ_{i1} and displacement field u_{01} of rock mass unit under the first unloading $\sigma_{\Delta i1}(u_{\Delta i1})$ are calculated and which was superimposed with the initial stress (displacement) field as Eq. (1).

$$\begin{cases}\sigma_{i1}=\sigma_0+\sigma_{\Delta i1}\\ u_{i1}=u_{\Delta i1}\end{cases} \tag{1}$$

Step 3: The variation values of the mechanical parameters of the rock mass unit are calculated and these mechanical parameters will be modified according to the value of unloading.

Step 4: The stress increment $\sigma_{\Delta in}$ and the displacement increment $u_{\Delta in}$ of the *n*-th unloading are calculated at first. Then the stress field $\sigma_{i(n-1)}$ and the displacement field $u_{\Delta i(n-1)}$ are superimposed with the *n*-th unloading as Eq. (2).

$$\begin{cases}\sigma_{in}=\sigma_{i(n-1)}+\sigma_{\Delta in}\\ u_{in}=u_{i(n-1)}+u_{\Delta in}\end{cases} \tag{2}$$

So, the stress and displacement values of the excavated rock in the unloading zones under certain unloading conditions can be obtained by Eq. (2).

3.2. MECHANICAL PARAMETERS CALCULATION AND UNLOADING ZONES

Assuming that the unloading time is long enough, the unloading state of each step can be regarded as consistent with the initial elastic state and the stress-strain relation obeys the generalized Hooke's law as Eq. (3).

$$\begin{cases}\Delta\varepsilon_1=\dfrac{1}{E}\left[\Delta\sigma_1-\mu\left(\Delta\sigma_2+\Delta\sigma_3\right)\right]\\ \Delta\varepsilon_2=\dfrac{1}{E}\left[\Delta\sigma_2-\mu\left(\Delta\sigma_1+\Delta\sigma_3\right)\right]\\ \Delta\varepsilon_3=\dfrac{1}{E}\left[\Delta\sigma_3-\mu\left(\Delta\sigma_1+\Delta\sigma_2\right)\right]\end{cases} \tag{3}$$

Where $\Delta\sigma_i$ (i=1, 2, and 3) is the unloading stress component (MPa), and $\Delta\varepsilon_i$ (i=1, 2, and 3) is the unloading strain component, respectively. E and μ are the elastic modulus (GPa) and Poisson ratio.

According to Eq. (3), the calculating formula of Poisson ratio μ and elastic modulus E can be deduced as follows:

$$\mu=\frac{\Delta\sigma_2\Delta\varepsilon_1-\Delta\sigma_1\varepsilon_2}{\left(\Delta\sigma_3+\Delta\sigma_1\right)\Delta\varepsilon_1-\left(\Delta\sigma_2+\Delta\varepsilon_3\right)\Delta\varepsilon_2} \tag{4}$$

$$E=\frac{\Delta\sigma_3-\mu\left(\Delta\sigma_1+\Delta\sigma_2\right)}{\Delta\sigma_3} \tag{5}$$

The Mohr's circle can be drawn by the stress values in different stress states caused by the numerical calculation. And through the envelope line of the Mohr's circle, the equivalent strength of internal friction angle and cohesion of the surrounding rock after the tunnel excavation can be derived as Eqs. (6) and (7).

$$\varphi_i=\sin^{-1}\left[\frac{\left(\sigma_1^{'}-\sigma_3^{'}\right)-\left(\sigma_1-\sigma_3\right)}{\sigma_1^{'}+\sigma_3^{'}-\left(\sigma_1+\sigma_3\right)}\right] \tag{6}$$

$$c_i=\frac{\left(\sigma_1-\sigma_3\right)-\left(\sigma_1+\sigma_3\right)\sin\varphi_i}{2\cos\varphi_i} \tag{7}$$

Where $\sigma_1^{'}$ and $\sigma_3^{'}$ are the secondary stress (MPa), σ_1 and σ_3 are the initial stress (MPa).

In elastic theory, assuming that the surrounding rock of a tunnel generally extends the distance at infinity, so it is generally considered that the excavation influence zones are infinite. However, as for the practical engineering, only the obvious changing zones caused by the unloading stress and displacement can have an significant influence on the tunnel stability. Thus the influence zones can be regarded as where the stress values of these zones are larger than that of the initial stress zones, which can be equal to the excavation unloading belt. This can be expressed by Eq. (8).

$$\left|\sigma'-\sigma_0\right|\geq\lambda\sigma_0 \tag{8}$$

Where σ' is the secondary stress component (MPa), σ_0 is the initial stress component (MPa), and λ is the perturbation factor.

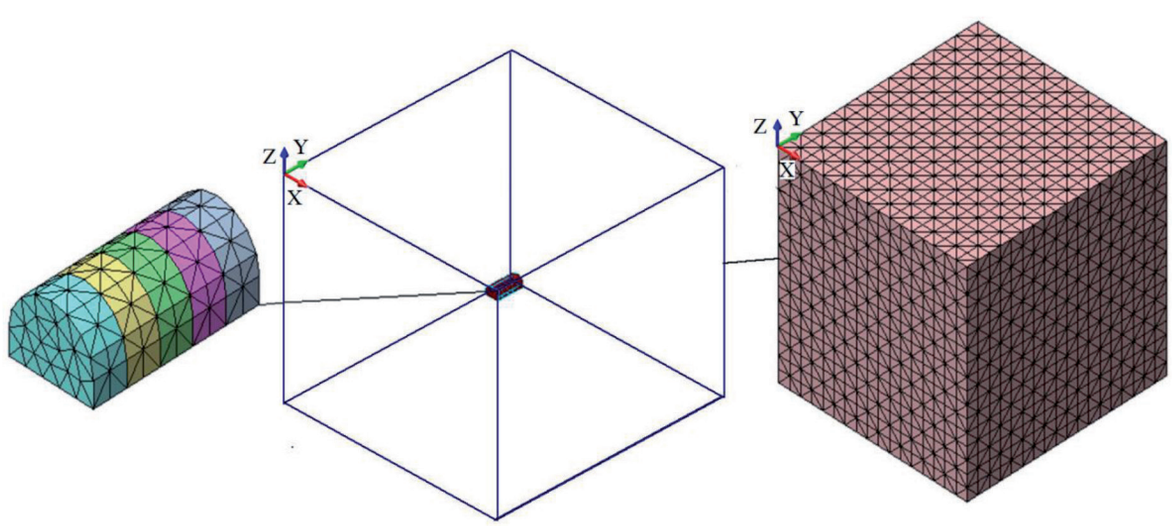

Fig. 2: The computational model and its meshes

Name	Density (Kg/m^3)	Elastic modulus (GPa)	Poisson ratio	Cohesion (MPa)	Internal friction angle (°)	Tensile strength (MPa)
Carboniferous sandstone	2600	5.00	0.22	3.80	40	1.50

Table I: Physical and mechanical parameters of the model

The unloaded belt is where the stress value is greater than or equals to that of the specific value of the perturbation factor.

3.3. THE COMPUTATIONAL MODEL AND SIMULATION METHOD

Taking Shimen Mine in China as the engineering background, the buried depth of the tunnel was about 850 m. The shape of the tunnel was straight wall with half arch and the excavation section was 4.8 m wide and 3.9 m high. The surrounding rock of the tunnel was main carboniferous sandstone.

As shown in Fig. 2, the three-dimension computational model was built by using MIDAS/GTS technique (MIDAS Information Technology Co., Ltd.; Geotechnical and Tunnel analysis syetem). The computational model was 90 m long (*Y*-axis), 85 m wide (*X*-axis), and 84 m high (*Z*-axis), respectively. The mesh was progressive with refinement and the model was automatically divided into 17623 elements. The rock above the top of the model was converted into the vertical load applied on the model as the vertical stress boundary. The horizontal stress was calculated according to the in-situ stress inversion. The horizontal displacements of four lateral boundaries of the model were restricted, and the bottom of the model was fixed. The physical and mechanical parameters of the model were listed in Table I. The surrounding rock behavior was assumed to follow the Mohr-Coulomb strength criterion.

The tunnel was located in the center of the model. The simulation excavation length of the tunnel was 10 m long, and the whole section was excavated completely in one time with excavation length of 2.0 m by each step. So the excavation process was divided into five steps.

4. RESULTS AND DISCUSSION

4.1. DETERMINING UNLOADING ZONES OF SURROUNDING ROCK

As shown in Fig. 3 (Unloading zones of the surrounding rock in the displacement field along the *Y*-axial direction, See section: supplementary material at the end of this article), with the increase of the excavation length, the deformation area of the surrounding rock was basically not expanding along the *Y*-axial direction. The changing range of the *Y*-displacement was about 8.0 m, and which was divided into three zones. Zone 1 represented the obvious deformation and the range was about 2.0 m, and its displacement was 7-11 mm. Zone 2 was the median deformation and the range was around 3.0 m, and its displacement was 4-7 mm. Zone 3 displayed low deformation and the range was around 3.0 m, and its displacement was 1-4 mm.

As shown in Fig. 4 (Unloading zones of the surrounding rock in the stress field along the *Y*-axial direction, See section: supplementary material), with the increase of the excavation length, the stress area of the surrounding rock was about 7.0 m along the *Y*-axial direction, and which was divided into four zones. The variation of ranges and stresses were listed in Table II.

As shown in Fig. 5 (Unloading zones of the surrounding rock in the stress field along the X-axial direction, See section: supplementary material), after the tunnel excavation, the changing range of the *X*-stress was about 10 m along *X*-axial, and which was divided into three zones. The changing range of the tunnel vault was about 3.0 m along *Z*-axial, and which was divided into two zones. Similarly, the changing range of the tunnel floor along

Zone	Zone range (m)	Stress value after excavation (MPa)	Initial stress value (MPa)	Chang percentage (%)
1	1.0	0.77-14.05	31.60	55.54-97.56
2	1.0	14.05-18.91	31.60	40.16-55.54
3	1.5	18.91-23.7	31.60	25.00-40.16
4	3.5	23.7-31.05	31.60	1.74-25.00

Table II: Analysis of unloading zones in the stress field along the Y-axial direction

Zone		Zone range (m)	Stress value after excavation (MPa)	Initial stress value (MPa)	Chang percentage (%)
Left wall	1	2.0	23.70-36.50	55.10	33.76-56.99
	2	3.0	36.5-45.10	55.10	18.15-33.76
	3	5.0	45.11-53.60	55.10	2.72-18.15
Right wall	4	2.0	23.70-36.50	55.10	33.76-56.99
	5	3.0	36.50-45.10	55.10	18.15-33.76
	6	5.0	45.11-53.60	55.10	2.72-18.15
Vault	7	1.0	70.80-79.30	55.10	28.94-43.92
	8	2.0	79.30-92.10	55.10	43.92-67.51
Floor	9	1.0	70.80-79.30	55.10	28.94-43.92
	10	2.0	66.50-70.80	55.10	20.69-28.49

Table III: Analysis of unloading zones in the stress field along the X-axial direction

Zone		Zone range (m)	Stress value after excavation (MPa)	Initial stress value (MPa)	Chang percentage (%)
Left wall		5.0	13.30-19.80	21.10	10.43-36.97
Right wall		5.0	13.30-19.80	21.10	10.43-36.97
Vault		4.0	13.30-19.80	21.10	10.43-36.97
Floor	1.0	4.30-8.60	21.10	59.24-79.62	28.94-43.92
	2.0	8.60-13.30	21.10	36.97-59.24	43.92-67.51
	2.0	13.30-16.40	21.10	22.27-36.97	28.94-43.92
	2.0	16.40-18.90	21.10	10.43-22.27	20.69-28.49

Table IV: Analysis of unloading zones in the stress field along the Z-axial direction

Z-axial was about 3.0 m, and which was also divided into two zones. The variation of ranges and *X*-stress values were listed in Table III.

As shown in Fig. 6 (Unloading zones of the surrounding rock in the stress field along the *Z*-axial direction, See section: supplementary material), after the tunnel excavation, the changing range of the *Z*-stress was about 5.0 m along *X*-axial, and which was divided into one zone. The changing range of the tunnel vault was about 4 m along *Z*-axial, and which was divided one zone. Similarly, the changing range of the tunnel floor was about 4.0 m along *Z*-axial, and which was divided into four zones. The variation of ranges and *Z*-stress values were listed in Table IV.

To sum up the above arguments, after the tunnel excavation, the uploading zones around the tunnel were generalized and divided into three zones, namely I, II, and III as shown in Fig. 7.

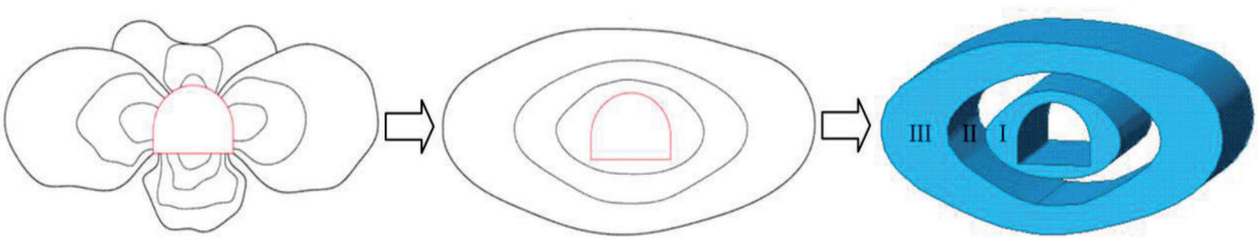

Fig. 7: Unloading zones of the surrounding rock of the tunnel

4.2. DETERIORATION LAWS OF THE MECHANICAL PARAMETERS

With the increase of the tunnel excavation length along *Y*-axial, the mechanical parameters of the surrounding rock in different unloading zones were gradually deteriorating and these unloading zones were also increased gradually. So it was necessary to adjust the ranges of these unloading zones and these mechanical parameters during the process of the tunnel excavation. It was proposed that each unloading load would be 10 % of the initial stress, and the equilibrium state would be achieved when the unloading load was about 50-60 % of the initial stress. Then, the computational model was divided into six calculation steps, and each step would be reversely uploaded 4.4 MPa (*X*-axial), 2.2 MPa (*Y*-axial) , and 2.0 MPa (*Z*-axial), respectively. Since the mechanical parameters influencing the tunnel stability were mainly cohesion, internal friction angle, elastic modulus and Poisson ratio, the changing rules of these four mechanical parameters in different unloading zones were analyzed during the excavation process of the tunnel. The stress and strain in three unloading zones were calculated at each excavation step, and these change values of the mechanical parameters in the different unloading zones were obtained by Eqs. (3) to (7).

4.2.1. Characteristics of internal friction angle variation

As seen from Table V (See section: supplementary material), with the increase of the tunnel excavation length of the tunnel, the internal friction angle of the unloading zones I, II and III had been gradually decreased, respectively. The change tendency of internal friction angle in the unloading zones I, II and III was from urgent to slow. The Zone I where the parameter changed obviously, and the internal friction angle was about 50 % of the initial value, which was equivalent to the loose belt of the surrounding rock of the tunnel. The Zone II was a moderate variation region, and the internal friction angle was about 60 % of the initial value, which was equivalent to the plastic belt of the surrounding rock of the tunnel. The Zone III was a low variation region, and the internal friction angle was about 77 % of the initial value, which was equivalent to the elastic belt of the surrounding rock of the tunnel.

The deteriorating rules of the internal friction angle in different unloading zones were concluded based on these data in Table V (See section: supplementary material) by using Matlab software, and the internal friction angle η_φ fitting functions were as these formulas (9) to (11).

The internal friction angle fitting function in Zone I, Zone II, and Zone III were Eqs. (9) to (11), respectively.

$$\eta_\varphi = -0.0005\alpha^3 + 0.0178\alpha^2 + 0.2058\alpha + 1.1866, \quad R^2 = 0.9957 \quad (9)$$

$$\eta_\varphi = 0.0014\alpha^3 - 0.0138\alpha^2 - 0.0432\alpha + 1.049, \quad R^2 = 0.9924 \quad (10)$$

$$\eta_\varphi = 0.0014\alpha^3 - 0.0149\alpha^2 - 0.0010\alpha + 1.0116, \quad R^2 = 0.9906 \quad (11)$$

Where α is the uploading step.

4.2.2. Characteristics of cohesion variation

As seen from Table VI (See section: supplementary material), with the increase of the tunnel excavation length of the tunnel, the cohesion of the unloading zones I, II and III had been gradually decreased also, respectively. According to statistic, the cohesion in zone I was about 43 % of the initial value, and the cohesion in

zone II was about 58 % of the initial value, and the cohesion in zone III was about 68 % of the initial value.

The deteriorating rules of the cohesion in different unloading zones were concluded based on these data in Table VI (See section: supplementary material) by using Matlab software, and the cohesion η_c fitting functions were as these formulas (12) to (14).

The cohesion fitting function in Zone I, Zone II, and Zone III were Eqs. (12) to (14), respectively.

$$\eta_c = -0.0045\alpha^3 + 0.0506\alpha^2 + 0.2721\alpha + 1.2182, \quad R^2 = 0.9898 \quad (12)$$

$$\eta_c = -0.0025\alpha^3 + 0.0249\alpha^2 + 0.1492\alpha + 1.1273, \quad R^2 = 0.9998 \quad (13)$$

$$\eta_c = 0.0010\alpha^3 - 0.0177\alpha^2 + 0.0150\alpha + 1.0000, \quad R^2 = 0.9953 \quad (14)$$

4.2.3. Characteristics of elastic modulus variation

As seen from Table VII (See section: supplementary material), with the increase of the tunnel excavation length of the tunnel, the elastic modulus of the unloading zones I, II and III had been gradually decreased also, respectively. According to statistic, the elastic modulus in zone I was about 51 % of the initial value, and the elastic modulus in zone II was about 60 % of the initial value, and the elastic modulus in zone III was about 74 % of the initial value.

The deteriorating rules of the elastic modulus in different unloading zones were concluded based on these data in Table VII (See section: supplementary material) by using Matlab software, and the elastic modulus η_E fitting functions were as these formulas (15) to (17).

The elastic modulus fitting function in Zone I, Zone II, and Zone III were Eqs. (15) to (17), respectively.

$$\eta_E = 0.0023\alpha^3 - 0.0173\alpha^2 + 0.0739\alpha + 1.0870, \quad R^2 = 0.9985 \quad (15)$$

$$\eta_E = 0.0006\alpha^3 - 0.0050\alpha^2 - 0.0716\alpha + 1.0761, \quad R^2 = 0.9995 \quad (16)$$

$$\eta_E = 0.0008\alpha^3 - 0.0102\alpha^2 - 0.0157\alpha + 1.0254, \quad R^2 = 0.9975 \quad (17)$$

4.2.4. Characteristics of Poisson's ratio variation

As seen from Table VIII (See section: supplementary material), with the increase of the tunnel excavation length of the tunnel, the Poisson's ratio of the unloading zones I, II and III had been gradually increased, respectively. According to statistic, the Poisson's ratio in zone I was about 120.1 % of the initial value, and the Poisson's ratio in zone II was about 110.8 % of the initial value, and the Poisson's ratio in zone III was about 104.8 % of the initial value.

The deteriorating rules of the Poisson's ratio in different unloading zones were concluded based on these data in Table VIII (See section: supplementary material) by using Matlab software, and the Poisson's ratio η_μ fitting functions were as these formulas (18) to (20).

The Poisson's ratio fitting function in Zone I, Zone II, and Zone III were Eqs. (9) to (11), respectively.

$$\eta_\mu = -0.0005\alpha^3 + 0.0049\alpha^2 + 0.0276\alpha + 0.9683, \quad R^2 = 0.9996 \quad (18)$$

$$\eta_\mu = -0.0011\alpha^3 + 0.0108\alpha^2 + 0.0026\alpha + 0.9933, \quad R^2 = 0.9997 \quad (19)$$

$$\eta_\mu = -0.0001\alpha^3 + 0.0008\alpha^2 + 0.0080\alpha + 0.9913, \quad R^2 = 0.9999 \quad (20)$$

4.3. CONVENTIONAL ANALYSIS COMPARED WITH UNLOADING CALCULATION TO SUPPORTING

For the sake of contrast, the supporting model of the tunnel (Fig. 8) was built and the mechanical response of the supporting were obtained by comparing the conventional analysis with the unloading calculation. The main supporting parameters were listed in Table IX (See section: supplementary material).

As seen from Table X (See section: supplementary material), for the unloading zone of the surrounding rock of the tunnel, the maximum displacement 20 mm occurred at the lateral wall and the vertical displacement 10 mm occurred at the floor by the conventional analysis. While considering the unloading effect, the maximum displacement was 55 mm in *X*-axial direction, which increases by 1.75 times compared with the conventional analysis. And the vertical displacement was 31 mm in *Y*-axial direction, which was increased by 2.10 times compared with the conventional analysis. Moreover, for the shotcrete lining of the tunnel, the maximum displacement 20 mm occurred at the lateral wall and the vertical displacement 4.3 mm occurred at the arch by the conventional analysis. While considering the unloading effect, the maximum displacement was 54 mm in *X*-axial direction, which increases by 1.70 times compared with the conventional analysis. And the vertical displacement was 12 mm in *Y*-axial direction, which was increased by 1.79 times compared with the conventional analysis. For the unloading zone of the surrounding rock of the roadway, the maximum stress 159 MPa occurred at the arch and the vertical stress 40 MPa occurred at the lateral wall by the conventional analysis. While considering the unloading effect, the maximum stress was 276 MPa in *X*-axial direction, which increases by 0.73 times compared with the conventional analysis. And the vertical stress was 76 MPa in *Y*-axial direction, which was increased by 0.90 times compared with the conventional analysis.

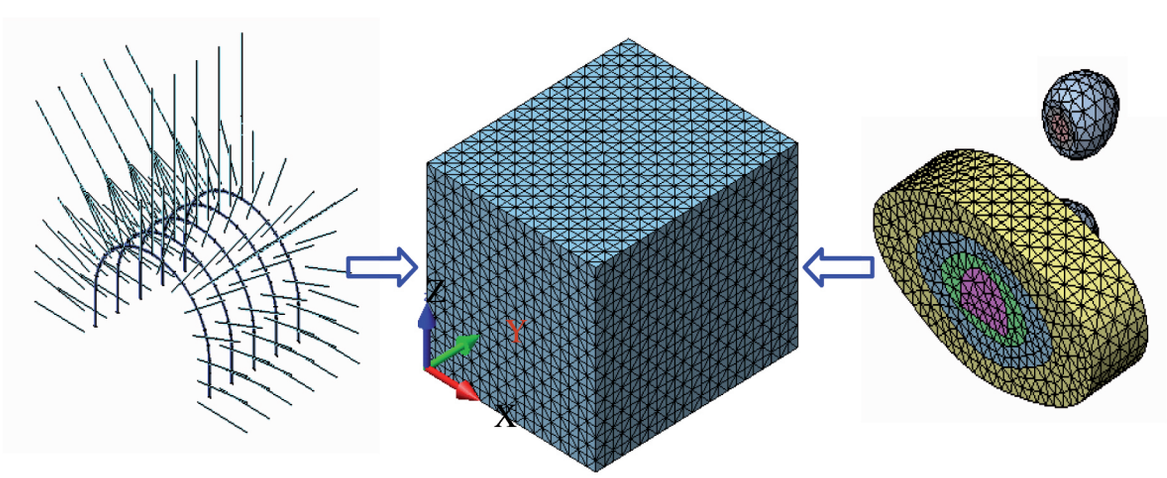

Fig. 8: The supporting model of the tunnel

As seen from Table XI (See section: supplementary material), for the shotcrete lining of the tunnel, the maximum stress 159 MPa occurred at the roof and the vertical stress 67 MPa occurred at the arch by the

conventional analysis. While considering the unloading effect, the maximum stress was 340 MPa in *X*-axial direction, which increases by 1.14 times compared with the conventional analysis. And the vertical stress was 124 MPa in *Y*-axial direction, which was increased by 0.85 times compared with the conventional analysis.

As seen from Table XII (See section: supplementary material), for the force of the rock bolt, the maximum force was 218 kN by the conventional analysis. While the maximum force was 591 kN considering the unloading effect, which increased by 1.71 times compared with the conventional analysis. For the force of the steel support, the maximum force was 3000 kN in *X*-axial direction and the vertical force was 6.1 kN in *Z*-axial direction by the conventional analysis. While the maximum force was 6480 kN in *X*-axial direction considering the unloading effect, which increased by 1.16 times compared with the conventional analysis. The vertical force was 13 kN in *Z*-axial direction, which increased by 1.13 times compared with the conventional analysis.

From Table X to XII (See section: supplementary material), it can be found that the increasing range of the mechanical response index, such as displacement, stress and force, increased about 0.73-2.10 times comparing the conventional analysis with the unloading calculation. So the unloading effect can not be ignored for the numerical calculation of the deep tunnel excavation.

CONCLUSIONS

To reveal the mechanical parameters deterioration rules of the surrounding rock for the deep tunnel excavation, based on the background of the deep tunnel in Shimen Mine in China, the three-dimension computational model was built by using MIDAS/GTS technique, and the deformation and failure mechanism of the tunnel excavation considering unloading effect was analyzed. The main conclusions were obtained as follows:

(1) The excavation unloading belt formula was put forward, and the different unloading zones of the surrounding rock were determined after the deep tunnel excavation according to the formula.

(2) It is found that the mechanical parameters for the different unloading zones, such as cohesion, internal friction angle, elastic modulus, and Poisson's ratio, displayed the nonlinear degradation characteristics.

(3) The unloading effect had a great influence on the stress field, the displacement field, and the forces of the supporting after the tunnel excavation. So it was more important to consider the unloading effect for the deep tunnel excavation.

In this study, the surrounding rock of the deep tunnel was close to hard brittle rock. However, it was not clear whether there would be a large variability under the soft rock conditions. Moreover, since the time factor was not taking into consideration in the elastic analysis, for the engineering practice, the time factor should be taken into consideration by a different approach for the creep behavior in the further study.

BIBLIOGRAPHY

[1] Yin DP. "Selection of the mining methods for the high seam adopted in the Xingdian coalmine". Sci/Tech Information Development & Economy. April 2005. Vol. 15-15, p. 274-275.

[2] Li JL, Wang LH. "Study on size effect of unloaded rock mass". Chinese Journal of rock mechanics and engineering. December 2003. Vol. 22-11, p. 2032-2036.

[3] Varas F, Alonso E, Alejano LR, et al. "Study of bifurcation in the problem of unloading a circular excavation in a strain-softening material". Tunnelling and Underground Space Technology. July 2005. Vol. 20-4, p. 311-322. DOI: http://dx.doi.org/10.1016/j.tust.2004.12.003

[4] Cai M, Kaiser PK. "Assessment of excavation damaged zone using a micromechanics model". Tunnelling and Underground Space Technology. July 2005. Vol. 20-4, p. 301-310. DOI: http://dx.doi.org/10.1016/j.tust.2004.12.002

[5] Malmgren L, Saiang D, Toyra J, et al. "The excavation disturbed zone (EDZ) at Kiirunavaara mine, Sweden-by seismic measurements". Journal of Applied Geophysis. January 2007. Vol. 61-1, p. 1-15. DOI: http://dx.doi.org/10.1016/j.jappgeo.2006.04.004

[6] Kwon S, Lee CS, Cho SJ, et al. "An investigation of the excavation damaged zone at the underground research tunnel in Korea". Tunnelling and Underground Space Technology. January 2009. Vol. 24-1, p. 1-13. DOI: http://dx.doi.org/10.1016/j.tust.2008.01.004

[7] Wassermann J, Sabroux JC, Pontreau S, et al. "Characterization and monitoring of the excavation damaged zone in fractured gneisses of the Rose lend tunnel, French Alps". Tectonophysics. April 2011. Vol. 503-1, p. 155-164. DOI: http://dx.doi.org/10.1016/j.tecto.2010.10.013

[8] Fattahi H, Farsangi MAE, Shojaee S, et al. "Selection of a suitable method for the assessment of excavation damage zone using fuzzy AHP in Aba Saleh Almahdi tunnel, Iran". Arabian Journal of Geosciences. May 2015. Vol. 8-5, p. 2863-2877. DOI: http://dx.doi.org/10.1007/s12517-014-1280-7

[9] Siren T, Kantia P, Rinne M. "Considerations and observations of stress-induced and construction-induced excavation damage zone in crystalline rock". International Journal of Rock Mechanics and Mining Sciences. January 2015. Vol. 73, p. 165-174. DOI: http://dx.doi.org/10.1016/j.ijrmms.2014.11.001

[10] Song L, Li HZ, Chan CL, et al. "Reliability analysis of underground excavation in elastic-strain-softening rock mass". Tunnelling and Underground Space Technology. November 2016. Vol. 60, p. 66-79. DOI: http://dx.doi.org/10.1016/j.tust.2016.06.015

[11] Rahal S, Sellier A, Casaux-Ginestet G. "Poromechanical consolidation and basic creep interactions around tunnel excavation". International Journal of Rock Mechanics and Mining Sciences. April 2017. Vol. 94, p. 55-63. http://dx.doi.org/10.1016/j.ijrmms.2016.12.009

[12] Qian QH. "The characteristic scientific phenomena of engineering response to deep rock mass and the implication of deepness". Journal of East China Institute of Technology. March 2004. Vol. 27-1, p. 1-5.

[13] Xie HP, Ju Y, Li LY. "Criteria for strength and structural failure of rocks baded on energy dissipation and energy release principles". Chinese Journal of rock mechanics and engineering. September 2005. Vol. 24-17, p. 3003-3010.

[14] Wang MY, Zhou ZP, Qian QH. "Tectonic deformation and failure problems of deep rock mass". Chinese Journal of rock mechanics and engineering. April 2006. Vol. 25-3, p. 448-455. DOI: http://dx.doi.org/10.3321/j.issn:1000-6915.2006.03.002

[15] Gu JC, Gu LY, Chen AM, et al. "Model test study on mechanism of layered fracture within surrouding rock of tunnels in deep stratum". Chinese Journal of rock mechanics and engineering. March 2008. Vol. 27-3, p. 433-438. DOI: http://dx.doi.org/10.3321/j.issn:1000-6915.2008.03.001

[16] Wu WP, Feng XT, Zhang CQ, et al. "Classification of failure modes and controlling measures for surrounding rock of deep tunnel in hard rock". Chinese Journal of rock mechanics and engineering. September 2011. Vol. 30-9, p. 1782-1802.

[17] Li J, Song CM, Hu X, et al. "Analysis of deformation and failure mechanism of surrounding rock for deep underground projects". Rock and Soil Mechanics. November 2012. Vol. 33-S2, p. 365-370.

[18] Liu XX, Liang ZZ, Zhang YB, et al. "Unloading test for rock burst mechanism in tunnel model". Journal of Engineering Geology. November 2016. Vol. 24-5, p. 967-975. DOI: http://dx.doi.org/10.13544/j.cnki.jeg.2016.05.028.

ACKNOWLEDGEMENTS

This work was financially supported by the National Natural Science Foundation of China (51774112; 51474188; 51074140), the Doctoral Fund of Henan Polytechnic University (B2015-67), 2015 Australian Endeavour Research Fellowship and Taihang Scholars Program. All these are gratefully appreciated.

SUPPLEMENTARY MATERIAL

http://www.revistadyna.com/documentos/pdfs/_adic/8554-1.pdf